Proceedings of the Estonian Academy of Sciences,
2019, **68**, 2, 131–139
https://doi.org/10.3176/proc.2019.2.02
Available online at www.eap.ee/proceedings

MATERIALS ENGINEERING

Production of metal–ceramic lattice structures by selective laser melting and carburizing or nitriding

Yaroslav Holovenko[a*], Lauri Kollo[a], Marek Jõeleht[a], Roman Ivanov[a], Tetiana Soloviova[b], and Renno Veinthal[a]

[a] Department of Mechanical and Industrial Engineering, Tallinn University of Technology, Ehitajate tee 5, 12611 Tallinn, Estonia
[b] Faculty of Physical Engineering, National Technical University of Ukraine "Igor Sikorsky Kyiv Polytechnic Institute", Peremohy Av. 37, 03680 Kyiv, Ukraine

Received 31 January 2019, accepted 19 February 2019, available online 28 March 2019

Abstract. Selective Laser Melting (SLM) allows obtaining light-weight cellular lattice structures with complex geometry. However, producing metal–ceramic components, as well as cellular lattice structures, by SLM is limited. The present study focuses on obtaining metal–ceramic lattice structures by a two-step approach: SLM and post-processing. Nitriding and carburizing were applied to stainless steel cellular lattice structures. A set of post-processing parameters is estimated in order to nitridize and carburize metallic cellular lattice structures. Compared to the initial material, post-processed lattices exhibited higher average Vickers hardness values, measured for nitrided and carburized structures at 605 and 576 HV0.3, respectively, while the reference microhardness of steel 316L is 210 HV0.3. The highest average compressive yield strength value for untreated lattice was 60.7 MPa and for carburized lattices, 99.3 MPa.

Key words: selective laser melting, lattice structure, ceramic, nitriding, carburizing.

1. INTRODUCTION

Additive manufacturing enables to produce parts of complex shape directly from metal powder. The unique feature of this technique is the possibility of creating three-dimensional (3D) architected cellular lattice structures with properties determined by the structure and geometry of the object rather than by its composition [1,2].

Advanced ceramics are a group of materials that have high hardness with the temperature and corrosion resistance needed for many engineering applications. Production of ceramics by additive manufacturing has attracted great interest due to difficulties faced in processing complex objects by classical powder metallurgy methods, especially in small batch sizes. Another distinct benefit is the low demand for post-processing, as ceramic materials are hard to machine. Producing ceramic and metal–ceramic shapes or cellular lattice structures has been found difficult to be achieved by direct printing methods [3]. High cooling rates during the process give rise to thermal stresses, and due to the brittle nature of ceramics, tend to cause cracks in end products [4]. Instead of direct 3D printing, ceramic parts are more commonly produced by using indirect methods, where organic binders and ceramic particles are mixed and shaping is performed by polymer printing methods such as fused deposition modelling, selective laser

* Corresponding author, yaholo@taltech.ee

sintering, or binder jetting. In these cases an additional sintering step is required. Such approach allows producing ceramics with near full density and high mechanical performance [5,6]. Another indirect approach uses the polymer pyrolysis route for obtaining ceramic parts [7]. Eckel et al. [8] reported a successful attempt at obtaining a ceramic cellular lattice structure with fine detail size using the stereolithography process for forming the polymer. Pyrolysis was applied as post-processing in order to form ceramic structures [8]. The limitation of such an approach is the restricted number of ceramics that can be obtained by this route. A similar two-step approach can be applied also to metal lattice structures. A well-known method for creating protective metal–ceramic composite layers on metal surfaces is case hardening, mainly through nitriding [9,10], or carburizing [11]. When such treatments are applied to thin lattice structures, the maximal penetration depth can be higher than the size of the lattice strut diameter. Therefore, it can be assumed that all-directional influence on the strut will lead to changes in the material with a minimal gradient. Post-treatment increases hardness, strength, wear resistance, load carrying capability, and fatigue strength.

The aim of the present study was to introduce and estimate a new processing route for metal–ceramic composite lightweight cellular lattice structures by combining selective laser melting and thermochemical treatment. Metal–ceramic lattices produced by the presented approach may also have an advantage over metallic ones in thermoacoustic applications due to the changed thermal properties of the material.

2. EXPERIMENTAL

2.1. Materials

The cellular lattice structures were produced from atomized AISI 316L powder delivered by Shijiazhuang Daye Metal Powder Factory. The particle size was in the range from 10 to 45 μm. The chemical composition of stainless steel 316L powder is presented in Table 1.

2.2. Lattice generation

Lattices were created using RDesigner software developed by Realizer GmbH. The lattice geometry is represented as a beam model. A modified octet truss unit cell (Fig. 1a) was used in this study. All horizontal elements were removed from the initial octet truss unit cell due to pulsed laser scanning strategy limitation. Samples with the dimensions of 10 mm × 10 mm × 15 mm were produced (Fig. 1b). The unit cell size was varied from 1 mm to 1.47 mm. A set of lattice structures was chosen in order to investigate the influence of thermochemical treatment with minor changes in relative density.

Table 1. Chemical composition of AISI 316L

Alloying element	Content, wt%
Fe	Rest
C	<0.03
Cr	16–18.5
Ni	10–14
Mo	2–3
Mn	<2
Si	<1
P	<0.045
S	<0.03

2.3. Selective Laser Melting (SLM) process and post-processing

All the printing experiments were performed on a Realizer SLM50 selective laser melting machine. Pulsed laser scanning strategy was employed to obtain lattices. The laser current was kept constant at 4000 mA, which is approximately equal to 100 W laser power. The exposure time (ET) was varied from 400 μs to 1100 μs. During the process nitrogen was used as a protective atmosphere, and the oxygen level was kept at less than 0.2%. Hot isostatic pressing (HIP) and carburizing were used as post-processing procedures. HIP was used in order to perform the nitriding of lattice structures with applying overpressure. HIP was carried out at 1150 °C at 100 MPa under nitrogen. Carburizing was performed in CH_4 flow of 250 ccm under atmospheric pressure at 1000 °C for 20 min, which was followed by dwelling in furnace under vacuum at 1150 °C for 1 hour.

2.4. Measurements and characterizations

Structural investigations of the lattices were performed by using Scanning Electron Microscope (SEM) Hitachi TM1000 and Zeiss Evo MA15. In order to investigate microstructural changes, specimens were embedded inside a polymer matrix, ground, and polished. Compressive strength of the lattice structures was measured at a loading rate of 1 mm/min, using the Instron 8516 servo-hydraulic testing system. X-ray diffraction (XRD) was carried out on a Rigaku Ultima IV machine with a Cu Kα beam and measuring step width of 0.05°. A Buehler Micromet 2001 microhardness tester was used for Vickers hardness measurements with the load of 300 gf.

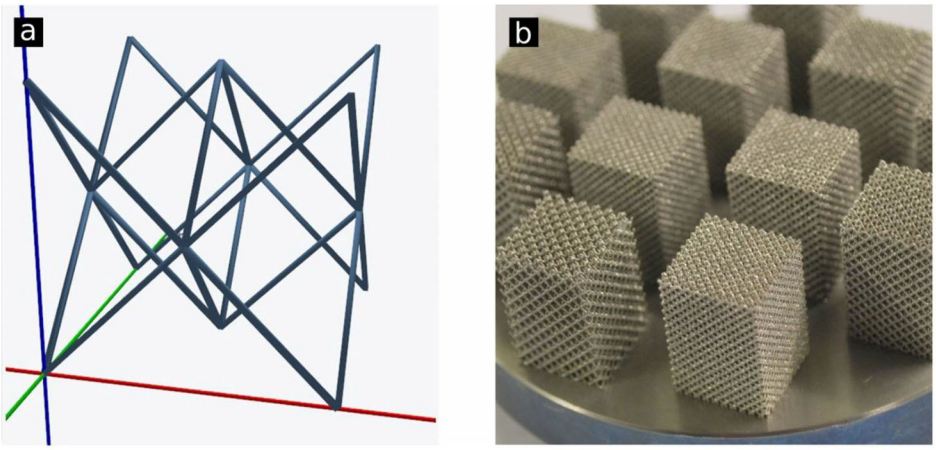

Fig. 1. Beam model of the lattice unit cell (a) and image of produced lattice structures (b).

3. RESULTS AND DISCUSSION

3.1. Morphology and relative density of the lattices

The SEM image of the 3D printed lattice structure obtained at the lowest exposure time (ET = 400 μs) clearly shows that a number of bonded particles are connected to the downface side of oblique struts whereas their top surface is relatively smooth (Fig. 2). The highest exposure time (ET = 1100 μs) caused longer existence of the liquid phase and higher thermal influence on the surrounding unmelted powder (Fig. 2b). As a result, the downface surface of lattice struts is covered with a significant number of bonded particles and waves caused by solidified inflows of molten material in overhanging regions. The strut diameter increased with the exposure time.

Due to the presence of an inclination angle, certain phenomena were observed. First of all, some of the molten material overhung the previous solid layer. This molten material had been pulled down by gravity and particles located underneath became connected to the strut surface. A similar phenomenon was observed by Suard et al. [12] and Yan et al. [13]. At the same time, particles located under the oblique strut can be partially melted or sintered due to thermal flux specifics during the SLM process [14].

According to the Gibson–Ashby model, the strength and modulus of the porous cellular lattice structure depend on the ratio of lattice density to bulk material density [15]. In this study, the relative density of the obtained lattice structures varied from 14.85% to 41.14%; these values are related to the lattice densities

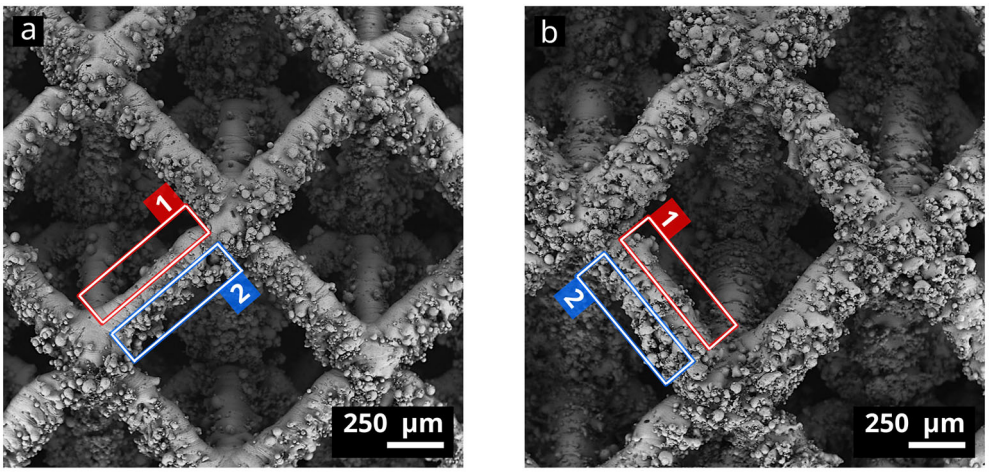

uus-ok

Fig. 2. Octet truss lattice structure obtained at ET 400 μs (a) and at ET 1100 μs (b); 1 – upper side and 2 – downface side of the oblique strut surface.

of 1.19 g/cm^3 and 3.29 g/cm^3, respectively. The smallest relative density values were obtained for lattices with 1.47 mm unit cell size, and the highest for 1 mm unit cell size. Table 2 provides relative densities of lattices.

3.2. Microstructure

Cross-sections specific at different heights of the lattice are illustrated in Fig. 3. The node of the lattice is the place of struts interconnection. Usually locations of nodes correspond to unit cell vertexes. The cross-sections in the places located close to a node are characterized by a larger area compared to the cross-section of a single strut. This leads to local differences in post-processing conditions. However, thermochemical treatment is all-directional and the penetration depth is larger than the element size. The approximate penetration depth of up to 0.6 mm in the case of nitriding [16] and up to 1 mm for carburizing [17] can be achieved under conditions similar to those used in this work. The sizes of the lattice elements were smaller than the mentioned penetration depth, which provides full transformation of the whole lattice volume into the metal–ceramic composite.

Additionally, some geometrical irregularities were present at the bottom of the node area. These are related to bonded particles below the struts. Also, close proximity of laser exposure points leads to material sintering between them. The cross-sections of the lattice nodes after nitriding and carburizing are represented in Fig. 4a and 4d, respectively. In Fig. 4a, it is visible how individual struts start detaching from the node. In these places crack-like spacing appears.

The main feature of the carburization process in this study was the occurrence of a gas flow, which could theoretically cause the presence of a deposition gradient. In previous works [18,19] the deposition of a graphene layer on the bundle of ceramic nanofibres was observed. In case of nanofibres, gas penetration inside the sample was challenged by the fact that the distance between fibres was around 20–50 nm. The deposition gradient was found to be present for the specimens over 3 cm in length and the gas flow more than 500 ccm. In the case of the lattices, the porosity was much higher, but specimen sizes and gas flow were two times below the reported values. The microstructures of nitrided and carburized lattices were characterized by the absence of any significant gradient in the phase distribution. This shows that the penetration depth during the thermo-chemical treatment was sufficient through the whole cross-section of struts. Several phases were evenly distributed through the cross-section when the initial material was a one-phase alloy.

The microstructure of the nitrided lattice consisted of three phases: matrix (marked as N-1A) and two types of inclusions (marked as N-1B for an average linear size of 0.86 µm and as N-1C for 0.32 µm size (shown in Fig. 4b)). Visual representation of Energy-Dispersive X-ray Spectroscopy (EDS) data is shown in Fig. 4c

Table 2. Relative densities of the lattices

Exposure time [µs]	Relative density [%]			
	Unit cell size [mm]			
	1	1.11	1.26	1.47
600	28.8 ± 0.3	24.8 ± 0.3	19.9 ± 0.2	14.9 ± 0.5
800	34.1 ± 0.4	27.5 ± 0.5	23.3 ± 0.3	15.8 ± 0.6
1100	41.1 ± 0.3	32.6 ± 0.4	24.7 ± 0.4	19.6 ± 0.4

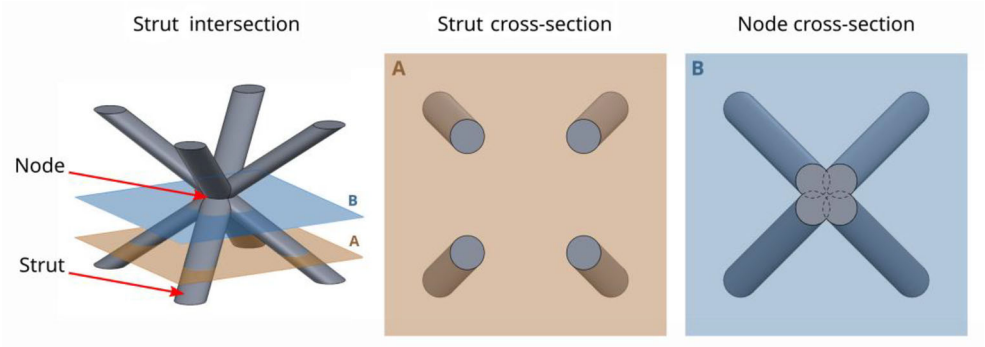

Fig. 3. Schematic illustration of cross-sections specific to different places of the lattice.

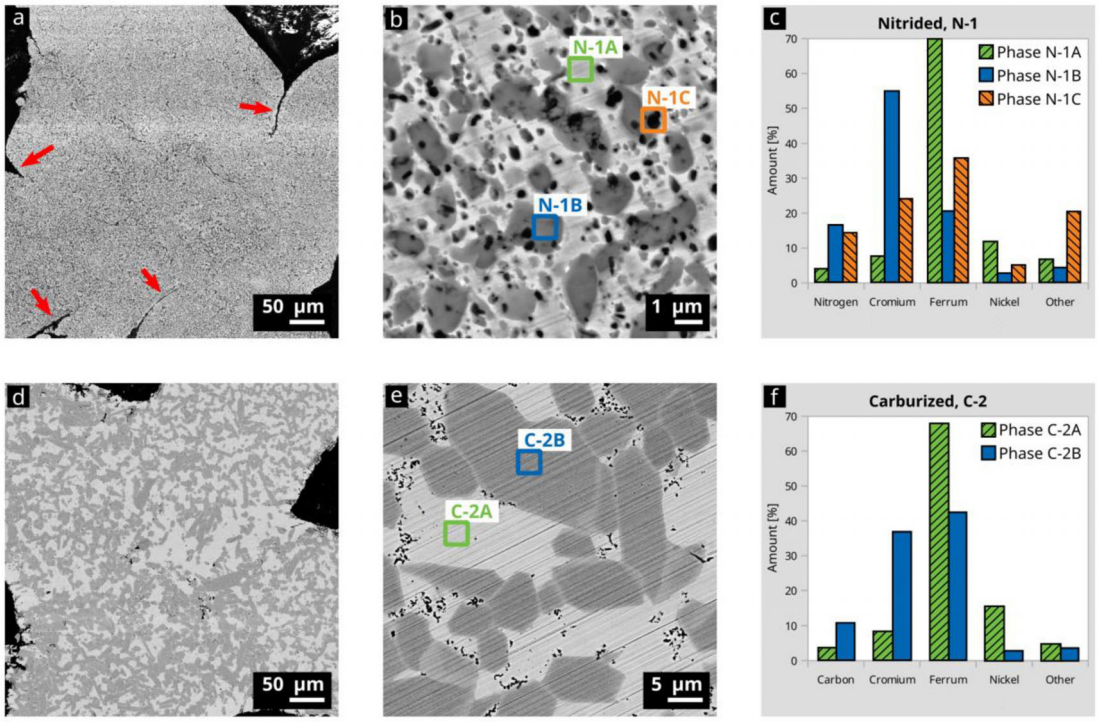

Fig. 4. SEM micrographs and EDS results of nitrided (a, b, c) and carburized (d, e, f) lattices. Arrows point to crack-like spacing.

and 4f. The size of the N-1C phase is always less than 1 µm, resulting in inaccurate EDS analysis since it also includes information about the surrounding phases. The XRD results provide evidence of chromium nitride in the sample as well as iron nitride (Fig. 5a). The XRD patterns of pure 316L powder do not exhibit such additional peaks [20]. Considering also EDS results, it can be concluded that during the HIP process chromium and iron form nitrides resulting in a multiphase metal–ceramic lattice structure.

The microstructure of the carburized lattice consists of two main phases: C-2A and C-2B (Fig. 4e). Compared to nitrided lattices, the C-2B phase showed significantly larger sizes averaging at 12.3 µm. In combination with XRD results (Fig. 5b), it can be concluded that chromium tended to form carbides. Black dots in the microstructure

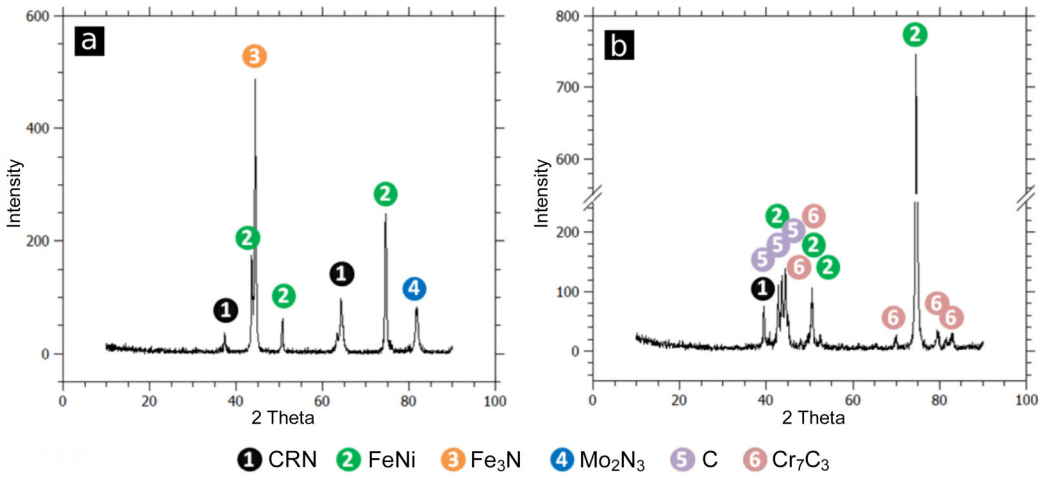

Fig. 5. XRD patterns for nitrided (a) and carburized (b) lattices.

are microscopic voids (Fig. 4e), which are located on the interfacial boundaries. The size of the single pore was less than 1 µm. The main possible reason of the formation of voids is the so-called diffusion porosity or Kirkendall and Frenkel effect [21]. Chromium diffuses faster than iron or nickel [22], it also tends to form carbides first. Vacancies formed by the migration of Cr atoms cannot be fulfilled by atoms of other elements with the same speed. Therefore, pores are forming in such a specific location as the interfacial boundaries. The presence of carbon peaks in Fig. 5b can be attributed to the residual deposited graphite on the surface.

3.3. Microhardness and mechanical properties

The average microhardness of nitrided lattices was 605 HV0.3 and of carburized lattices, 576 HV0.3. Vickers hardness of the bulk SLM processed virgin AISI 316L was measured at 210 HV0.3. These results are in good agreement with the values reported in the literature [23–25]. Figure 6 shows strength characteristics of lattices. Compressive yield strength tended to grow with relative density (Fig. 6a). The obtained results, in general, correlate with the Gibson–Ashby model [15]. The calculated coefficient of correlation $R = 0.9865$. Nevertheless, it is also clear that experimental data slightly differ from the compressive yield strength estimated by the Gibson–Ashby model. As was concluded in [13], the differences in theoretical and experimentally tested values can be attributed to the residual stress and more complex geometry caused by bonded particles. Nitrided and carburized lattices became brittle and collapsed at some point of testing (Fig. 6c, 6d) while the untreated stainless steel lattices did not collapse at all during the testing up to 50% of deformation when the test stopped due to the programmed limit. The average ultimate fracture strength of carburized and nitrided lattices with relative density in the range of 19.6–24.7% was comparable. However, with increasing relative density values, the difference in strength became more

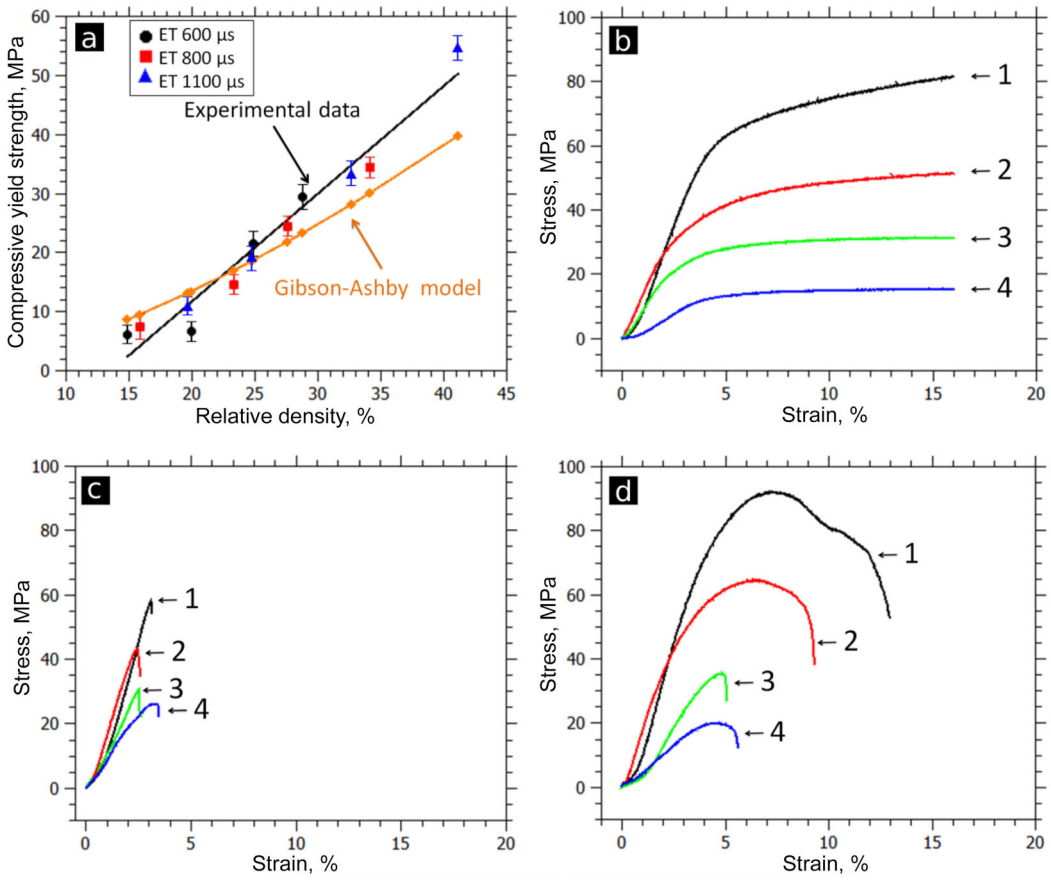

Fig. 6. Measured and calculated according to the Gibson–Ashby model compressive yield strength values of untreated lattices vs relative density (a) and stress–strain curves for untreated (b), nitrided (c), and carburized (d) lattices. Relative densities: 1 – 41.1%, 2 – 32.6%, 3 – 24.7%, 4 – 19.6%.

noticeable. Lattices with relative density of 41.1% showed compressive ultimate strength (fracture stress) of carburized lattices about 1.5 times as high as nitrided lattices. Nitrided lattices exhibited 2–3% deformation in the elastic zone before collapsing without plastic deformation. In the case of carburized lattices, some plastic deformation was observed. Deformation for carburized lattices before critical failure was from about 4.5% to 8% for lattices with the lowest and with the highest relative density, respectively (Fig. 6d). Lower plasticity of nitrided structures is caused by the peculiarities of the structure of the nitrided layer. In general, the nitrided structure may be divided into two sublayers: a compound zone and a nitrogen diffusion zone [10,16], both consisting of the nitrides Fe_3N and Fe_4N phase. The Fe_2-Fe_3N phase (detected by XRD in the current case) is known to be hard but very brittle. Carburized layers usually contain some amount of the metallic phase (ferrite or austenite) in their structure, which provides them a relatively high plasticity.

Table 3 summarizes compressive yield strength, fracture stress, and elastic modulus of untreated lattices as well as nitrided and carburized lattices. Compressive yield strength of carburized lattices increased on average by 10 MPa over the whole range of lattice relative densities. With the increasing of the lattice relative density, the difference between the yield strength and the fracture stress increased. Compressive yield strength values are not available for nitrided lattices because of the absence of the yield point (0.2% offset line did not cross the strain–stress curve). The fracture occurred in the linear elastic region. Elastic modulus increased with density (Table 3). Post-processing tended to increase the elastic modulus.

Further research could be focused on wear properties of such metal–ceramic lattices. Regular metal as printed lattices has a stable coefficient of friction and exhibits wear debris removal by the self-cleaning effect due to the ordered geometry and designed porosity lattices [26]. An increase of wear resistance is expected after post-processing. One more study direction could be application of metal–ceramic lattice structures as a porous acoustic material [27] with predefined geometry. Their application as stacks [28] for thermoacoustic energy harvesting [29] is expected to be more efficient compared with the use of stacks produced by traditional manufacturing or similar lattices made from metal. Post-treatment of metallic lattices resulted in phase transformation and, as a consequence, change of thermal and acoustic properties.

4. CONCLUSIONS

In this study metal AISI 316L lattices were produced by selective laser melting and post-processed by thermochemical treatment in methane and nitrogen. The following conclusions can be drawn:

- Nitriding and carburizing transformed the metallic lattice structure into a metal–ceramic composite material.
- Hardness increased about three times compared to untreated specimens in both cases.
- Compressive yield strength of carburized lattices increased on average 10 MPa, which corresponds to 21–65% increase depending on lattice density. The elastic modulus increased on average in the range from 16% to 46%.
- Carburized lattices were found to be more efficient than nitrided ones due to their higher strength and slightly higher plasticity with comparable hardness.

ACKNOWLEDGEMENTS

This study was supported by the Estonian Ministry of Education and Research (IUT 19-29; base funding provided to R&D institutions, project B56); the personal grant of the Estonian Research Council (PUT1063); the European Regional Development Fund, project number 2014-2020.4.01.16-0183 (Smart Industry Centre); and ASTRA 'TUT Institutional Development Programme for 2016–2022' Graduate School of Functional Materials and Technologies (2014-2020.4.01.16-0032). The publication costs of this article were covered by the Estonian Academy of Sciences.

Table 3. Results of compressive test

Lattice relative density [%]	Compressive yield strength [MPa]		Ultimate fracture stress [MPa]		Elastic modulus [GPa]		
	Untreated	Carburized	Nitrided	Carburized	Untreated	Nitrided	Carburized
19.6	10.95	18.5	27	21	0.42	0.96	0.59
24.7	19.2	30	31.2	33	1.08	1.25	1.10
32.6	33.35	42	44.6	69	1.51	2.2	1.95
41.1	54.8	66.7	60.7	99.3	1.76	2.33	2.31

REFERENCES

1. Yan, C., Hao, L., Hussein, A., and Raymont, D. Evaluations of cellular lattice structures manufactured using selective laser melting. *Int. J. Mach. Tool. Manu.*, 2012, **62**, 32–38.
2. Yang, L. Experimental-assisted design development for a 3D reticulate octahedral cellular structure using additive manufacturing. *Rapid Prototyping J.*, 2015, **21**(2), 168–176.
3. Shishkovsky, I., Yadroitsev, I., Bertrand, Ph., and Smurov, I. Alumina-zirconium ceramics synthesis by selective laser sintering/melting. *Appl. Surf. Sci.*, 2007, **254**, 966–970.
4. Davydova, A., Domashenkov, A., Sova, A., Movtchan, I., Bertrand, P., Desplanques, B., et al. Selective laser melting of boron carbide particles coated by a cobalt-based metal layer. *J. Mater. Process. Technol.*, 2016, **229**, 361–366.
5. Shahzad, K., Deckers, J., Zhang, Z., Kruth, J. P., and Vleugels, J. Additive manufacturing of zirconia parts by indirect selective laser sintering. *J. Eur. Ceram. Soc.*, 2014, **34**, 81–89.
6. Leu, M. C., Pattnaik, S., and Hilmas, G. E. Investigation of laser sintering for freeform fabrication of zirconium diboride parts. *Virtual Phys. Prototyp.*, 2012, **7**, 25–36.
7. Riedel, R., Mera, G., Hauser, R., and Klonczynsky, A. Silicon-based polymer-derived ceramics: synthesis properties and applications – a review. *J. Ceram. Soc. Jpn.*, 2006, **114**, 425–444.
8. Eckel, Z. C., Zhou, C., Martin, J. H., Jacobsen, A. J., Carter, W. B., and Schaedler, T. A. Additive manufacturing of polymer-derived ceramics. *Science*, 2016, **351**, 58–62.
9. Barrallier, L. Classical nitriding of heat treatable steel. In *Thermochemical Surface Engineering of Steels* (Mittemeijer, E. J. and Somers, M. A. J., eds). Woodhead Publishing, 2015, 392–411.
10. Van Wiggen, P. C., Rozendaal, H. C. F., and Mittemeijer, E. J. The nitriding behaviour of iron-chromium-carbon alloys. *J. Mater. Sci*., 1985, **20**, 4561–4582.
11. Edenhofer, B., Joritz, D., Rink, M., and Voges, K. Carburizing of steels. In *Thermochemical Surface Engineering of steels* (Mittemeijer, E. J and Somers, M. A. J., eds). Woodhead Publishing, 2015, 485–554.
12. Suard, M., Martin, G., Lhuissier, P., Dendievel, R., Vignat, F., Blandin, J. J., and Villeneuve, F. Mechanical equivalent diameter of single struts for the stiffness prediction of lattice structures produced by Electron Beam Melting. *Addit. Manuf.*, 2015, **8**, 124–131.
13. Yan, C., Hao, L., Hussein, A., Bubb, S. L., Young, P., and Raymont, D. Evaluation of light-weight AlSi10Mg periodic cellular lattice structures fabricated via direct metal laser sintering. *J. Mater. Process. Technol.*, 2014, **214**, 856–864.
14. Wauthle, R., Vrancken, B., Beynaerts, B., Jorissen, K., Schrooten, J., Kruth, J. P., and Van Humbeeck, J. Effects of build orientation and heat treatment on the microstructure and mechanical properties of selective laser melted Ti6Al4V lattice structures. *Addit. Manuf.*, 2015, **5**, 77–84.
15. Gibson, L. J. and Ashby, M. F. The mechanics of three-dimensional cellular materials. *Proc. R. Soc. A Math. Phys. Eng. Sci.*, 1982, **382**, 43–59.
16. Pye, D. *Practical Nitriding and Ferritic Nitrocarburizing*. ASM International, Materials Park, Ohio, 2003.
17. Parrish, G. *Carburizing: Microstructures and Properties*. ASM International, Materials Park, Ohio, 1999.
18. Hussainova, I., Ivanov, R., Stamatin, S. N., Anoshkin, I. V., Skou, E. M., and Nasibulin, A. G. A few-layered graphene on alumina nanofibers for electrochemical energy conversion. *Carbon*, 2015, **88**, 157–164.
19. Drozdova, M., Hussainova, I., Pérez-Coll, D., Aghayan, M., Ivanov, R., and Rodríguez, M. A. A novel approach to electroconductive ceramics filled by graphene covered nanofibers. *Mater. Des.*, 2016, **90**, 291–298.
20. Liu, Y., Yang, Y., Mai, S., Wang, D., and Song, C. Investigation into spatter behavior during selective laser melting of AISI 316L stainless steel powder. *Mater. Des.*, 2015, **87**, 797–806.
21. Wierzba, B. Competition between Kirkendall and Frenkel effects during multicomponent interdiffusion process. *Phys. A Stat. Mech. Appl.*, 2014, **403**, 29–34.
22. Rothman, S. J., Nowicki, L. J., and Murch, G. E. Self-diffusion in austenitic Fe-Cr-Ni alloys. *J. Phys. F Met. Phys.*, 1980, **10**, 383–398.
23. Tolosa, I., Garciandía, F., Zubiri, F., Zapirain, F, and Esnaola, A. Study of mechanical properties of AISI 316 stainless steel processed by "selective laser melting", following different manufacturing strategies. *Int. J. Adv. Manuf. Technol.*, 2010, **51**, 639–647.
24. Chang, C-N. and Chen, F-S. Wear resistance evaluation of plasma nitrocarburized AISI 316L stainless steel. *Mater. Chem. Phys.*, 2003, **82**, 281–287.
25. Muthukumaran, V., Selladurai, V., Nandhakumar, S., and Senthilkumar, M. Experimental investigation on corrosion and hardness of ion implanted AISI 316L stainless steel. *Mater. Des.*, 2010, **31**, 2813–2817.
26. Holovenko, Y., Antonov, M., Kollo, L., and Hussainova, I. Friction studies of metal surfaces with various 3D printed patterns tested in dry sliding conditions. *Proc. Inst. Mech. Eng. Part J J. Eng. Tribol.*, 2018, **232**, 43–53.
27. Auriemma, F. Study of a new highly absorptive acoustic element. *Acoust. Aust*., 2017, **45**, 411–419.
28. Swift, G. W. and Keolian, R. M. Thermoacoustics in pin-array stacks. *J. Acoust. Soc. Am.*, 1993, **94**, 941–943.
29. Avent, A. W. and Bowen, C. R. Principles of thermo-acoustic energy harvesting. *Eur. Phys. J. Spec. Top.*, 2015, **224**, 2967–2992.

Metall-keraamiliste võrestruktuuride valmistamine selektiivse lasersulatustehnoloogia ja nitreerimise ning karbidiseerimise teel

Yaroslav Holovenko, Lauri Kollo, Marek Jõeleht, Roman Ivanov,
Tetiana Soloviova ja Renno Veinthal

Selektiivne lasersulatustehnoloogia (SLM) võimaldab saada keerulise geomeetriaga kergeid võrestruktuure. Võimalused metall-keraamiliste komponentide ja võrestruktuuride tootmiseks SLM-tehnoloogia abil on siiski piiratud. Käesolevas uurimuses on keskendutud metall-keraamiliste võrestruktuuride saamisele kaheastmelise lähenemise abil, kasutades SLM-i ja järeltöötlust. Roostevabast terasest võrestruktuuridele rakendati nitreerimist ja karbidiseerimist, mille puhul hinnatakse järeltöötlusparameetrite komplekti mõju. Pärast võre töötlemist on Vickersi keskmised kõvaduse väärtused kõrgemad kui algmaterjalil. Vickersi kõvadus nitriiditud ja karbidiseeritud detailide puhul on vastavalt 605 ning 576 HV0.3, samas kui töötlemata 316L terase mikrokõvadus on 210 HV0.3. Suurim keskmine survetugevuse väärtus töötlemata võre puhul oli 60,7 MPa ja karbidiseeritud võre puhul 99,3 MPa.